Scripta Materialia 256 (2025) 116415

Contents lists available at ScienceDirect

Scripta Materialia

journal homepage: www.journals.elsevier.com/scripta-materialia

Developing neural networks to rapidly map crystallographic orientation using laser ultrasound measurements

Rikesh Patel *, Wenqi Li, Richard J. Smith, Matt Clark

Optics and Photonics Group, Faculty of Engineering, University of Nottingham, University Park, Nottingham, NG7 2RD, UK

ARTICLE INFO

Keywords:
Laser ultrasonics
Artificial neural network
Crystal structure
Microstructure
Non-destructive testing

ABSTRACT

Rapid measurement of crystal orientation is critical in the materials discovery process as it facilitates real-time decision-making and quality control. Acoustic inspection methods rapidly characterise microstructure without the need for extensive infrastructure or expense – the laser ultrasonic method known as Spatially Resolved Acoustic Spectroscopy (SRAS) has been developed with this intent and accurately characterises crystal orientation by leveraging a combination of forward modelling and an exhaustive brute force process to obtain the best-fit orientation. While effective, this method is computationally demanding and time-intensive. We introduce a novel approach that utilises neural networks to classify measured acoustic signals into orientation planes to significantly expedite the characterisation process and demonstrate classification on real-world Inconel 617 and CMX4 specimens. A reduction in the orientation determination time from around 10 hours (brute force search) down to 15 seconds (neural network) was achieved while exhibiting an average plane angle difference of between 5.3° and 13.8°.

The microstructure of crystalline materials fundamentally influences its macroscopic properties – the crystallographic arrangement, in particular the grain shape, size and orientation, dictates mechanical properties such as strength, ductility, and hardness, as well as electrical properties such as the conversion efficiency of silicon cells [1]. Changes in microstructure induced by processing, for example through heat treatment, can lead to alterations in the macroscopic behaviour, highlighting the inseparable connection between the micro and macro scales in materials science. Understanding and controlling material microstructure is pivotal for manufacturing tailored materials with desired properties.

Imaging the microstructure is the primary method used to evaluate material properties. Simple grain contrast maps can be created through a surface etch and optical imaging process, however, the full evaluation of mechanical properties cannot be obtained as the exact orientation of the grains is missing. Recent developments in measuring the direction of light from etched surfaces [2] or the polarisation state of the light [3] show promise as attempts to reclaim this information but suffer from large errors (often > 20° disorientation when compared with established planes) due to registration errors and fluctuating intensity measurements that are not decouplable from the orientation measurements. The prevailing method of crystallographic imaging instead measures diffraction patterns of radiated particles (electrons, X-ray, neutrons) as they pass through or are backscattered off different crystal structures and orientations. The gold standard of these measurement systems, electron backscatter diffraction (EBSD), boasts high inspection resolution, both spatially (~10 nm) and angular (~1°). While some state-of-the-art systems being developed use EBSD to map orientation in-situ during the processing of materials, including recrystallization [4] and deformation [5], it largely remains a post-process evaluation tool due to the system complexity, cost, and sample constraints.

Ultimately, the derived mechanical properties of polycrystalline materials rely on their elastic constants in relation to the constituent individual grain orientations. When considering the propagation of an acoustic wave through or on a material, the relation between crystal orientation and stiffness can be utilised, where the speed of the acoustic wave is dependent on the crystal orientation it is travelling through [6]. Primarily, ultrasonics are used to determine the single crystal elasticity values rather than for imaging the material microstructure based on them, largely due to the interrogation space of the techniques used – measurements can be obtained by measuring the bulk wave velocity through a single crystal, or more commonly by using Resonant Ultrasound Spectroscopy (RUS) which offers material coupling advantages [7]. However, it is possible to reduce the interrogation area of generated ultrasound using laser ultrasonics.

* Corresponding author at: University of Nottingham, NG7 2RD, UK.
E-mail address: rikesh.patel@nottingham.ac.uk (R. Patel).

https://doi.org/10.1016/j.scriptamat.2024.116415
Received 29 August 2024; Received in revised form 8 October 2024; Accepted 13 October 2024
Available online 17 October 2024

Spatially Resolved Acoustic Spectroscopy (SRAS) is a non-destructive laser ultrasound technique that both generates Surface Acoustic Waves (SAWs) and detects them on different materials [8]. The acoustic waves are thermo-elastically generated using a broadband pulsed laser through a grating pattern that has a fringe separation λ_g – this turns the SAW into a wave packet. While the speed of the acoustic wave changes with the material properties along the propagation path, the frequency f_s within the wave packet does not, and instead is entirely dependent on the material properties that dictate the wave speed only at the point of generation v_s and the incident laser fringe separation, such that $f_s = v_s/\lambda_g$. The frequency is measured using a second continuous wave laser and, either a simple knife edge detector if measurements are made on optically smooth surfaces, or a more complicated arrangement (Speckle Knife Edge Detector [9], Two Wave Mixing interferometer [10]) if measurements are made on rough surfaces. With a known material's elastic stiffness tensor and density, it is possible to calculate the SAW velocity given the local crystallographic orientation and relative wave propagation direction, or more usefully, SRAS can be used to measure the wave velocity at all angles at a single point (phase velocity) on the surface of a material and by using the material's elastic properties, it would be possible to determine the local crystallographic orientation [11]. However, due to this being an ill-defined problem, a brute force search algorithm is instead employed to find the best fit between the SAW phase velocity measurements made using SRAS and a complete set of calculated SAW phase velocities based on crystallographic planes – this is currently a computationally intensive and time-consuming task.

The development of artificial neural networks has led to them being used in a number of complex recognition tasks for large datasets. In particular, neural networks are often very useful in the categorisation of nonlinear and multidimensional data, and through iterative training can be made resilient to noisy and incomplete data. Machine learning algorithms have recently been utilised in materials inspection scenarios, including in ultrasonic non-destructive evaluation scenarios often to extract measurement signals from noisy waveforms [12] or for the processing or microstructural characterisations, often from EBSD imaging, to gain useful metrics or grain classification [13,14].

In this paper we present a neural network for the classification of crystallographic orientation using velocity surface measurements made by Spatially Resolved Acoustic Spectroscopy. The neural network developed is capable of producing Miller indices of individual inspection points (pixels) at a significantly higher speed than the currently used brute force search algorithm (BFSA) approach.

The SAW phase velocity at the different orientations of a single crystal is distinct for most of the crystal structures including cubic structures (i.e. nickel) – this can be utilised as a distinguisher to identify the crystal orientation and is calculated using the material's elastic constants (C_{ij}) and its mass density (ρ) [15]. However, depending on the orientation angle different modes of surface waves (e.g. Rayleigh wave, Pseudo-surface wave) have dominant amplitudes – the calculated SAW phase velocity database is created with this consideration. The brute force search algorithm (BFSA) exhaustively fits measured against calculated phase velocities via 2D cross-correlation – on a PC with Intel i7-950 (@2.8 GHz) CPU and 24 GB RAM, the orientation determination rate is ~40 pixels/sec.

The expectation of this study was that Machine Learning (ML) methodologies could be used to classify SAW phase velocity measurements into crystallographic orientation. As the resultant crystal planar values are known with respect to the theoretical SAW phase velocities, supervised learning, and specifically domain adaptive transfer learning can be employed to train a new neural network. Much like the currently employed BFSA, the newly developed algorithm will output discretised crystal planar values – this approach means that a simplified neural network structure can be developed. In comparison with larger models that may be unsupervised or self-learning, the AI model presented in this paper did not require multiple epochs for reinforcement training.

The training data was created using calculated cubic nickel SAW phase velocity values based on crystal planes in Miller indices form {hkl} – as this model includes equivalences in lattice symmetries, all measurable planes can be represented by iterating through the first two Miller indices. Therefore, the calculated training dataset consisted of a 21 × 21 × 180 matrix where the first two elements represented the crystals Miller indices from (001) to (111), with the third element containing the SAW or pseudo-SAW velocities with peak amplitudes in 1° increments up to 180° (given that at there is at least two-fold symmetry in elasticity values, and therefore SAW wave speed, in all crystal systems). Since it is not known at which angle the SRAS measurements would be made relative to the underlying plane, the dataset was extended to include all variations of possible measurements by circularly shifting through all elements. The SAW phase velocity measurements acquired using SRAS can be tuned to collect at any rotational increment – typically this is set to 10° as a good compromise between measurement speed and error on determined angular output [16]. For the final step in preparing the training dataset, the number of peak SAW values is reduced to 18 out of the 180 initially calculated at 10° angular steps to make up the features of the training data. Generally neural network layers can either be fully connected (FCNN) or more sparingly connected via convolution functions (CNN) – having convolutional layers allows for more flexibility in learning but requires large datasets for training making them more suited to image classification for example [17]. However for the task identified in this paper, as there is a fixed physical link between the identifying features and the singular set of outputs they correspond to, the use of a fully connected (FC) neural network is justified. The neural network structure is bilayered with the first- and second-layer sizes equal to 18 and 441 respectively. The network uses a ReLU activation function between each FC layer to provide non-linearity without affecting positive data flow, and a Softmax function before the classification output of Miller index values due to its ability to provide a probability distribution for each output of this multi-class model.

To evaluate the performance of the conceived neural network, it underwent 5-fold cross-validation (against the original training dataset). The average validation accuracy across all folds was equal to 93.6%. Fig. 1a shows the confusion matrix for the trained network, which consists of an extensive 441 (21 × 21) classification planes, with the ordering of plane classes illustrated in Fig. 1b. While the majority of planes are correctly classified (blue pixels), the predominant locations of misclassification (red pixels) occur at the boundary of each h iteration and one k-l iteration off the true class (which would appear similar from a crystal plane perspective).

One of the great benefits of the SRAS system is its capability to scan large specimens non-destructively and robustly [8] – for this study, SRAS was used to collect SAW phase velocity measurements to assess the functionality of the presented neural network. The wave generation patch size was equal to 200 μm (giving an interrogation area of 100 μm [8]) with fringe spacing (wavelength) equal to 24 μm. A total of 18 *rotational* measurements were made (separated by 10° from 0°-180°) at *spatial* step sizes of 50 μm on a large grain Inconel 617 (Nickel superalloy) specimen to improve the image appearance in the presence of noise. Overall ~1.425M points of SAW phase velocity measurements were fed through both the brute force search algorithm (BFSA) and the fully connected neural network (FCNN) to output spatially resolved Miller indices. For visualisation, the resultant orientations were mapped akin to inverse pole figures as shown in Fig. 2a (determined by BFSA) and Fig. 2b (determined by FCNN). An enlarged area in both images is shown in Fig. 2c (BFSA) and Fig. 2d (FCNN). A comparative processed image of the same area (3x stitched) scanned using Electron BackScatter Diffraction (EBSD) is shown in Fig. 2e – the EBSD scan was conducted using a FEI Sirion 200 field-emission SEM system at *spatial* step sizes of 10 μm.

The large maps show good agreement between the BFSA and FCNN determined crystal orientation. In the enlarged FCNN image, some pixels within clearly identifiable grains are being noticeably classified differently from neighbouring pixels – this makes the image appear *noisier*

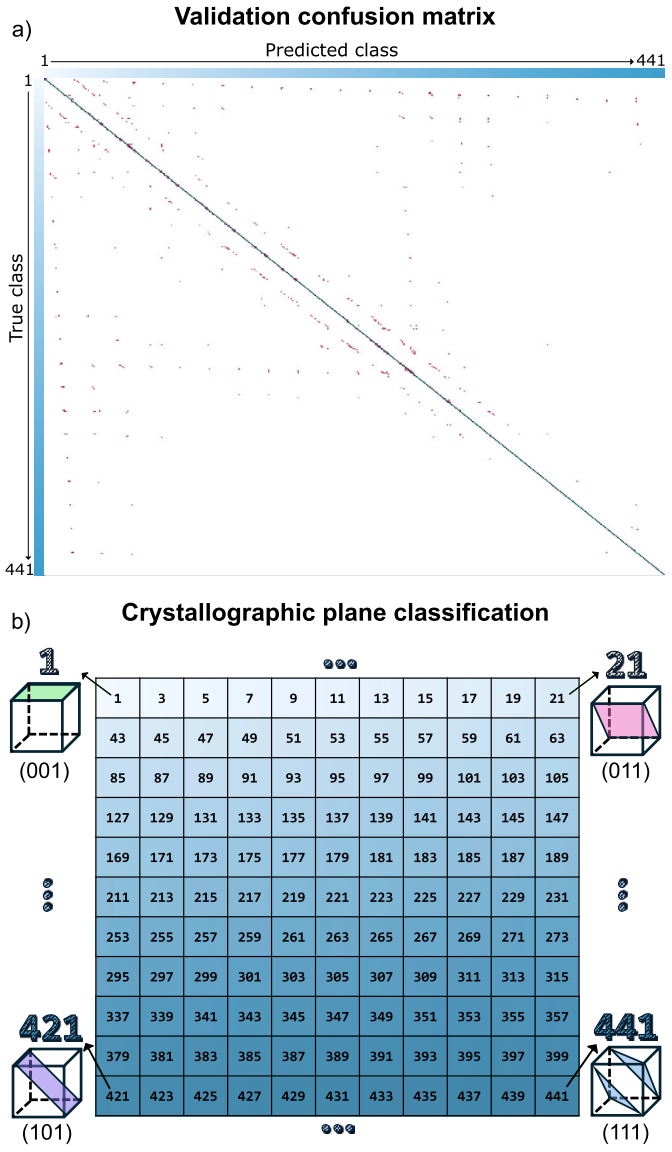

Fig. 1. a) The confusion matrix of the designed bilayer FCNN for Nickel: Input → FC → ReLU → FC → Softmax → Output. Correct classification is indicated by blue pixels, misclassification is indicated by red pixels. b) A schematic of the classification set number and its relation to all cubic crystallographic planes obtained through hkl iteration. Four representative (primary) planes are illustrated; class 1 is (001), class 21 is (011), class 421 is (101), class 441 is (111). (For interpretation of the colours in the figure(s), the reader is referred to the web version of this article.)

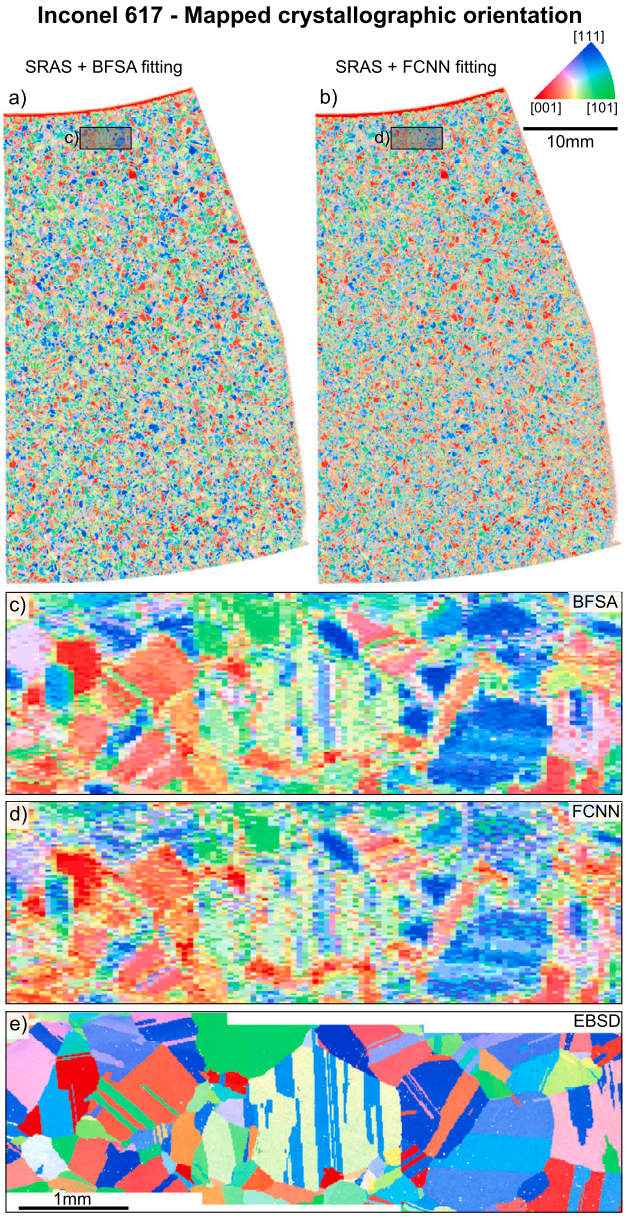

Fig. 2. Mapped crystallographic orientation of a large Inconel 617 specimen in Miller index using SRAS measurement data (50 μm step) as determined by a) BFSA and b) FCNN. A small section from the c) BFSA and d) FCNN enlarged for comparison with each other and with e) a (3x) stitched and processed EBSD scan of the same area (10 μm step).

than the BFSA determined image. The area of interrogation determines the SRAS measurement spatial resolution – while some grains are resolvable, locations where multiple smaller grains are present introduce orientation ambiguity in both fitting methods due to multiple SAW phase velocities being measured. This is also an issue at the boundaries of each large grain [8].

Despite this, features are broadly recognisable across all three images largely due to orientation (colour) similarity. As evident from the EBSD image, the advantage of scanning large samples using SRAS is that the sample does not require segmentation. The other advantage of using SRAS is the rapid scanning capability, where rather than operating over days to complete an EBSD scan, a physical SRAS scan would take hours. However the application of the BFSA fitting algorithm has been the current bottleneck in determining orientation — at 40 pixels/sec, 9.9 hrs was required for this image. In utilising the presented neural network, a determination speed of 90k pixels/sec was achieved, shortcutting the mapping of orientation down to 15.8 seconds.

With the Miller index values produced of the Inconel specimen by the BFSA and FCNN methods, the plane intersection angle difference θ_d relative to (001) can be calculated per pixel. Fig. 3 shows a histogram of the per-pixel angular difference when accounting for all pixels (red bars) – the absolute mean difference when considering all pixels is 13.8° with a standard deviation of 17.3°. By excluding boundary pixels from consideration (blue bars), the absolute mean difference decreases to 8.5° and the standard deviation to 12.7°.

To complement the results obtained from the Inconel specimen, the orientations of 10 different CMX4 (another nickel superalloy) single-crystal specimens were obtained using the Rolls Royce SCORPIO X-Ray Diffraction (XRD) system [18]. A table outlining the plane angular differences θ_d between the orientations determined between XRD measurements, the BFSA and FCNN methods are shown in Table 1. Given

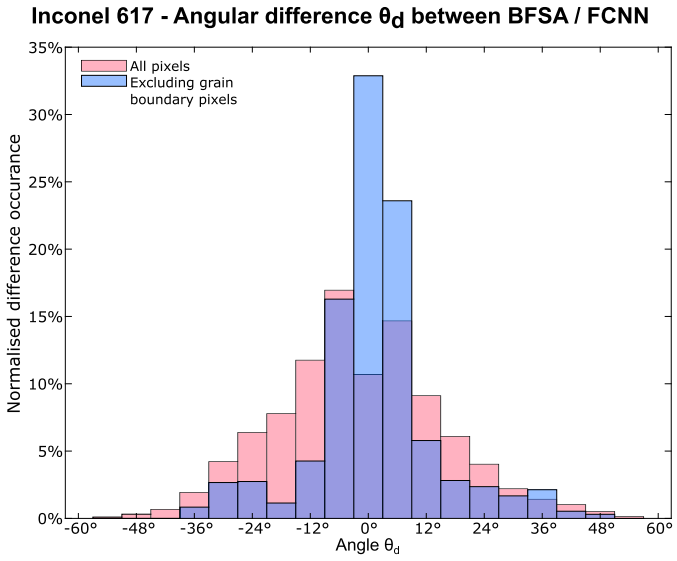

Fig. 3. Histogram showing plane intersection angle difference θ_d as determined between BFSA and FCNN methods of determining orientation from SAW phase velocities as captured using SRAS. The red bars consider all measurement pixels while the blue bars exclude boundary pixels as determined through Sobel edge detection (width 6px).

Table 1
Plane intersection angle differences θ_d relative to (001) of 10 different signal-crystal CMX4 (nickel superalloy) specimens as determined between XRD, BFSA and FCNN (using SRAS measurements). The absolute mean $|\bar{x}|$ and standard deviation σ between the three comparisons are also shown.

Sample No.	θ_d XRD vs BFSA	θ_d XRD vs FCNN	θ_d BFSA vs FCNN
01	4.61°	-4.07°	8.35°
02	3.03°	-7.01°	5.86°
03	3.81°	-9.07°	8.41°
04	-1.72°	-5.57°	-3.96°
05	-1.22°	-4.51°	4.03°
06	1.93°	-3.10°	3.87°
07	-3.08°	-5.80°	2.84°
08	9.91°	4.49°	6.25°
09	1.87°	-5.18°	2.83°
10	-4.14°	-9.28°	6.10°
$\|\bar{x}\|$	3.53°	5.81°	5.25°
σ	4.20°	3.87°	3.58°

that there are far fewer orientation ambiguities across all these specimens (single-crystal therefore no cross-boundary measurements), the absolute means $|\bar{x}|$ and standard deviations σ are much lower between all methods.

This paper has outlined a new approach in determining crystallographic orientation using surface acoustic wave phase velocity measurements as collected by the SRAS technique. A speed benefit of 2250× was achieved over the established brute force search and fitting algorithm as was demonstrated on a large (~30×50 mm) Inconel 617 specimen. Typically SAW velocity measurements can be obtained at speeds of up to 2000 points/sec, largely determined by the wave generating laser repetition rate [8] – with the Inconel specimen, a single direction velocity scan took 11.8 minutes to complete. Constructing the SAW phase velocity spectrum using 18 directional measurements took 3.5 hours. With the presented neural network, a complete SRAS orientation routine on this sample would be complete entirely within that 3.5 hours rather than taking over 13 hours when combining the time required for scanning and applying the BFSA method.

The focus of this study was to develop a small and simple proof-of-concept fully connected neural network for orientation determination of a single material – this achieved 93.6% validation accuracy which initially seems at odds when compared with the spread in angular difference between the FCNN and BFSA methodologies. An explanation for this could be that the signal-to-noise in the collected phase velocity spectra and the discrete nature of the neural network would lead some pixels to be incorrectly classified beyond what the validation accuracy would suggest – further investigation and improvement to the neural network would be required. However due to the reduced computational load in using the neural network for classification, both methods could be utilised sequentially to obtain complementary orientation results. Indeed, it is envisioned that such neural network architectures could be used to rapidly determine not only orientation for single materials, but to also determine the material itself from the velocity spectra alone (e.g. multi-material specimens), and to estimate material properties of unknown specimens such as its elasticity or phase.

CRediT authorship contribution statement

Rikesh Patel: Writing – review & editing, Writing – original draft, Software, Methodology, Investigation, Funding acquisition, Data curation, Conceptualization. **Wenqi Li:** Writing – review & editing, Writing – original draft, Visualization, Software, Methodology, Data curation, Conceptualization. **Richard J. Smith:** Writing – review & editing, Funding acquisition. **Matt Clark:** Writing – review & editing, Funding acquisition, Conceptualization.

Declaration of competing interest

The authors declare that they have no known competing financial interests or personal relationships that could have appeared to influence the work reported in this paper.

Acknowledgements

This work was supported by the Engineering and Physical Sciences Research Council [grant number EP/X000915/1]. E.ON Technologies is acknowledged for supplying the Inconel 617 specimen and Rolls Royce plc is acknowledged for supplying the CMX4 specimens and XRD measurements discussed in this paper. Bo Xiao from the University of Strathclyde is acknowledged for providing the EBSD scan data of the Inconel specimen.

References

[1] R. Patel, W. Li, R.J. Smith, S.D. Sharples, M. Clark, Orientation imaging of macro-sized polysilicon grains on wafers using spatially resolved acoustic spectroscopy, Scr. Mater. 140 (2017) 67–70, https://doi.org/10.1016/j.scriptamat.2017.07.003.
[2] X. Wang, S. Gao, J. Ekta, G. Bernard, S. Matteo, Measuring crystal orientation from etched surfaces via directional reflectance microscopy, J. Mater. Sci. 55 (2020) 11669–11678, https://doi.org/10.1007/s10853-020-04734-z.
[3] K. Jin, M. De Graef, c-Axis orientation determination of α-titanium using Computational Polarized Light Microscopy, Mater. Charact. 167 (2020) 110503, https://doi.org/10.1016/j.matchar.2020.110503.
[4] H.S. Ubhi, J. Parsons, N. Othen, S. Campbell, R. Poole, A. Gholinia, In-situ EBSD phase transformation and recrystallisation, J. Phys. Conf. Ser. 522 (2014) 012011, https://doi.org/10.1088/1742-6596/522/1/012011.
[5] R.M. Birch, J.O. Douglas, T.B. Britton, Characterization of local deformation around hydrides in Zircaloy-4 using conventional and high angular resolution electron backscatter diffraction, Mater. Charact. 202 (2023) 112988, https://doi.org/10.1093/micmic/ozad067.797.
[6] R.F.S. Hearmon, An Introduction to Applied Anisotropic Elasticity, Oxford University Press, 1961.
[7] M. Janovskaa, J. Nejezchlebova, P. Sedlak, T. Grabec, P. Stoklasova, J. Smilauerova, M. Janecek, S. Kratky, H. Seiner, Elastic constants of Ti-15Mo single crystals and their evolution with thermal treatment, MATEC Web Conf. 321 (2020) 12012, https://doi.org/10.1051/matecconf/202032112012.
[8] R.J. Smith, W. Li, J. Coulson, M. Clark, M.G. Somekh, S.D. Sharples, Spatially resolved acoustic spectroscopy for rapid imaging of material microstructure and grain

orientation, Meas. Sci. Technol. 25 (2014) 055902, https://doi.org/10.1088/0957-0233/25/5/055902.
[9] R. Patel, M. Hirsch, P. Dryburgh, D. Pieris, S. Achamfuo-Yeboah, R. Smith, R. Light, S. Sharples, A. Clare, M. Clark, Imaging material texture of as-deposited selective laser melted parts using spatially resolved acoustic spectroscopy, Appl. Sci. 8 (2018) 1991, https://doi.org/10.3390/app8101991.
[10] W. Li, P. Dryburgh, D. Pieris, R. Patel, M. Clark, R.J. Smith, Imaging microstructure on optically rough surfaces using spatially resolved acoustic spectroscopy, Appl. Sci. 13 (2023) 3424, https://doi.org/10.3390/app13063424.
[11] W. Li, S.D. Sharples, R.J. Smith, M. Clark, M.G. Somekh, Determination of crystallographic orientation of large grain metals with surface acoustic waves, J. Acoust. Soc. Am. 132 (2012) 738, https://doi.org/10.1121/1.4731226.
[12] S. Cantero-Chinchilla, P.D. Wilcox, A.J. Croxford, Deep learning in automated ultrasonic NDE – developments, axioms and opportunities, NDT E Int. 131 (2022) 102703, https://doi.org/10.1016/j.ndteint.2022.102703.
[13] E. Holm, R. Cohn, N. Gao, A.R. Kitahara, T.P. Matson, B. Lei, S.R. Yarasi, Overview: computer vision and machine learning for microstructural characterization and analysis, Metall. Mater. Trans. A 51 (2020) 5985–5999, https://doi.org/10.1007/s11661-020-06008-4.
[14] J. Pepper, O.L. Blanch, B. Thomas, M. Jacksone, Channelling electric current during the field-assisted sintering technique (FAST) to control microstructural evolution in Ti-6Al-4V, J. Mater. Sci. 58 (2023) 14514–14532, https://doi.org/10.1007/s10853-023-08884-8.
[15] G.W. Farnell, Properties of elastic surface waves, in: W.P. Mason, R.N. Thurston (Eds.), Physical Acoustics, vol. 6, Academic, New York, 1970, pp. 109–166.
[16] P. Dryburgh, R.J. Smith, P. Marrow, S.J. Lainè, S.D. Sharples, M. Clark, W. Li, Determining the crystallographic orientation of hexagonal crystal structure materials with surface acoustic wave velocity measurements, Ultrasonics (2020) 108–106171, https://doi.org/10.1016/j.ultras.2020.106171.
[17] M. Wittwer, M. Seita, A machine learning approach to map crystal orientation by optical microscopy, npj Comput. Mater. 8 (2022) 8, https://doi.org/10.1038/s41524-021-00688-1.
[18] A.T. Jones, C. Baxter, The Rolls Royce 'SCORPIO' system, Meas. Sci. Technol. 6 (1995) 131–133, https://doi.org/10.1088/0957-0233/6/1/021.